Deviational Monte Carlo scheme for thermal and electrical transport in metal nanostructures

Wuli Miao,[1] Yangyu Guo,[2] Xin Ran,[1] and Moran Wang[1,*]

[1]*Key Laboratory for Thermal Science and Power Engineering of Ministry of Education, Department of Engineering Mechanics and CNMM, Tsinghua University, Beijing 100084, China*

[2]*Institute of Industrial Science, The University of Tokyo, Tokyo 153-8505, Japan*

(Received 8 August 2018; revised manuscript received 18 February 2019; published 28 May 2019)

The electron is the dominant heat and charge carrier in metal, yet the Monte Carlo method for thermal and electrical transport remains not fully established due to the high density and high degeneracy of electrons. In this work, we develop a deviational Monte Carlo scheme to directly solve the Boltzmann transport equation for electron transport through a simplification of the full scattering term into relaxation time approximation form automatically including the Pauli exclusion principle. It is crucial to track the occupied and unoccupied electron states above and below the Fermi energy level, respectively, for Monte Carlo simulation of electron thermal transport. Our numerical scheme not only provides a clear physical picture, but also displays a good performance in predicting the temperature distribution, electronic thermal conductivity, and electrical conductivity for in-plane and cross-plane electron transport through metallic thin films. This work will promote the fundamental understanding of electron transport at micro- and nanoscale, and also provide a ground for the investigation of electron-phonon coupling transport.

DOI: 10.1103/PhysRevB.99.205433

I. INTRODUCTION

With the rapid development of nanoscience and nanotechnology in recent years, nanostructures and low-dimensional materials have drawn increasing attention due to their wide applications in thermoelectric conversion facilities, semiconductor electronic devices, etc. [1–3]. The metallic thin films play a significant role, as they are used as the interconnect materials in electronic circuits [4], the constituent of superlattice structure for thermoelectrics [5], and the efficient heat dissipation substrate for thermal management in micro- and nanoelectronics [6]. In these applications, the thermal and electrical properties of metallic thin film, which usually deviate from their bulk values, are the key to determine the performance and reliability of the whole system. Therefore, it is crucial to understand the thermal and electrical transport mechanism of metallic thin films at micro- and nanoscale.

Electrons are the dominant carriers of both heat and charge transport in metal although the contribution of phonons to thermal transport slightly increases at nanoscale [7–9]. Thus we focus on electron transport through metallic nanostructures in this work. The direct modeling of electronic thermal transport is often based on the kinetic theory of electrons [10]. The effective thermal conductivity of metallic thin films under the influence of external surface and/or grain boundary has been calculated based on a simple kinetic formula, with the effective electron mean free path (MFP) determined in a phenomenological way [11,12]. The MFP analysis will smear the detailed process of electronic heat transport, which has to recourse to the Boltzmann transport equation (BTE). The analytical solutions of electron BTE originally derived for electrical transport in metal nanostructures [13–15] have been extended to thermal transport in metallic nanothin films, nanowires, and nanoribbons [16–18]. However, these analytical models are usually applicable to simple structure geometries. A direct numerical solution of the electron BTE is indispensable for electron transport in more complex metallic nanostructures.

In comparison to the deterministic solver [19] (such as the discrete ordinates method [20]), the Monte Carlo scheme avoids a direct solution of the high-dimensional BTE based on the drift and collision of pseudoparticles, which further provides a more clear physical picture and an easier treatment of complex boundary condition. The ensemble Monte Carlo (EMC) scheme has been well developed and widely used in modeling electron transport in semiconductor nanostructures [21]. Unfortunately, it is not straightforward to adapt the EMC to model electron transport in metallic nanostructures due to the very different band structures and electron kinetics between metals and semiconductors [22]. Therefore, it is necessary to devise a Monte Carlo scheme specially for electron transport in metals, which rarely appears in the literature, to the authors' best knowledge. A Monte Carlo scheme has been given for numerical solution of the electron BTE to study the cross-plane electronic thermal transport through nanothin films [23–25]. Yet this Monte Carlo scheme remains to be improved due to the following two aspects: (i) it only considers the electrons at energy levels above the Fermi energy; (ii) the isothermal boundary condition is implemented by an empirical change of the scaling factor and the energy state of the computational particles. As a result, the temperature profile was obtained qualitatively without a solid validation whereas the heat flux calculation remains still unavailable [23–25].

*Corresponding author: mrwang@tsinghua.edu.cn

The main aim of this work is to promote the development of a Monte Carlo scheme for accurate prediction of electronic thermal transport in metallic nanostructures. We also consider the electrical transport by slightly adjusting the Monte Carlo scheme. Our work will contribute to not only a full account of electron states at energy levels both under and above Fermi energy, but also an appropriate treatment of the isothermal boundary with a heat bath method. In addition, we introduce the variance reduction technique recently developed in a deviational Monte Carlo scheme for rarefied gas flows [26] and nanoscale phonon transport [27]. The main idea of the deviational Monte Carlo scheme is to solve stochastically only the deviation of the distribution function from a referenced equilibrium distribution with the contribution from the latter part computed deterministically [26,27]. Thus the deviational Monte Carlo scheme can much reduce the computational burden and the stochastic uncertainties in contrast to the traditional Monte Carlo scheme. For the electron thermal transport in metals, the electron states deeply below the Fermi level are not influenced by the thermal perturbation due to the Pauli exclusion principle. Thus the deviational scheme is exceptionally significant by avoiding solving this part via subtracting a referenced equilibrium distribution.

The remaining of this article is organized as below. In Sec. II, the mathematical and numerical methodology is elaborated including the BTE for electron transport and the developed deviational Monte Carlo algorithm for thermal and electrical transport. In Sec. III, the Monte Carlo scheme is validated through modeling in-plane thermal and electrical transport and cross-plane heat transport through thin films. The concluding remarks are finally made in Sec. IV.

II. MATHEMATICAL AND NUMERICAL METHODOLOGY

A. Theoretical foundation

1. Electron BTE under relaxation time approximation

As long as the wave effect of electrons is negligible, the particle picture is appreciably valid for electron transport. The electron Boltzmann transport equation without magnetic field is expressed as [10]

$$\frac{\partial f}{\partial t} + \mathbf{v}\cdot\nabla_{\mathbf{r}} f - \frac{e\mathbf{E}}{\hbar}\cdot\nabla_{\mathbf{k}} f = C(f), \tag{1}$$

where $f \equiv f(\mathbf{r},\mathbf{k},t)$ is the electron distribution function denoting the electron occupation number around the wave vector $\mathbf{k}$ and the spatial position $\mathbf{r}$ at the moment t. $\hbar$ is the reduced Planck constant and $\mathbf{v}$ is the drift velocity relevant to electron energy. $\mathbf{E}$ is the external electric field. e is the element charge. At equilibrium state, f is given by the Fermi-Dirac distribution $f_0 = \{\exp[(\varepsilon-\mu)/k_B T]+1\}^{-1}$. The chemical potential μ is very close to the Fermi energy at the temperature scope studied in this work, thus $\mu = \varepsilon_F$ is assumed for the simplicity of mathematical description [22].

The collision term $C(f)$ evaluates the alteration of the distribution function from the electron scattering processes, and is written in a general form as

$$C(f) = \sum_{\mathbf{k}'} [f'(1-f)S(\mathbf{k}',\mathbf{k}) - f(1-f')S(\mathbf{k},\mathbf{k}')]. \tag{2}$$

The transition rate $S(\mathbf{k}',\mathbf{k})$ describes the probability of transition from one energy eigenstate ($\mathbf{k}'$) to another energy eigenstate ($\mathbf{k}$) of electron systems, when affected by a weak perturbation such as lattice vibration (phonons) and imperfection. It can be computed based on the Fermi's golden rule from the first-order perturbation theory [10,28–30]. The collision term $C(f)$ vanishes for equilibrium state yielding

$$(1-f_0)\sum_{\mathbf{k}'} f_0' S(\mathbf{k}',\mathbf{k}) = f_0 \sum_{\mathbf{k}'} (1-f_0') S(\mathbf{k},\mathbf{k}'). \tag{3}$$

Combined with the principle of detailed balance, Eq. (3) gives rise to

$$S(\mathbf{k},\mathbf{k}') = \exp\left(\frac{\varepsilon-\varepsilon'}{k_B T}\right) S(\mathbf{k}',\mathbf{k}). \tag{4}$$

In the linear response regime with weak deviation from equilibrium state, the electron distribution function can be written as $f(\mathbf{k}) = f_0 + f_1(\mathbf{k})$ with the deviation part a small quantity $f_1(\mathbf{k}) \ll f_0$. Under the relaxation time approximation (RTA) and also ignoring the high-order terms, we obtain the expression of relaxation time as

$$\frac{1}{\tau(\mathbf{k})} = \sum_{\mathbf{k}'} S(\mathbf{k}',\mathbf{k}) \left\{ f_0' + (1-f_0')\exp\left(\frac{\varepsilon-\varepsilon'}{k_B T}\right) - \frac{f_1'}{f_1}\left[1 - f_0 + f_0 \exp\left(\frac{\varepsilon-\varepsilon'}{k_B T}\right)\right]\right\}. \tag{5}$$

Apart from the prerequisite that electrons and lattices are sufficiently thermalized to be at the same local temperature [31], the RTA is valid only when the formula of τ is independent of the nonequilibrium process. First, we assume the phonon is in the local equilibrium state due to frequent scattering with electrons because of high electron density in metals. Then, the validity of RTA holds usually at two situations [31]: (i) isotropic electron scattering, and/or (ii) elastic electron scattering. Electron-phonon scattering and electron-imperfection scattering are the two main intrinsic sources of transport resistance in metals. We consider the ideal case of a pure metal without impurity in this work. The electron-acoustic phonon scattering is an inelastic process, since the energy of electrons is not conserved in the scattering process due to emitting or absorbing phonons. As a first step, the electron-phonon scattering is assumed to be isotropic, which represents a good approximation for electron heat transport around a temperature much higher than the Debye temperature considered in this work. Thus the relaxation time expression Eq. (5) of electrons becomes no longer dependent on the nonequilibrium distribution:

$$1/\tau(\mathbf{k}) = \sum_{\mathbf{k}'} S(\mathbf{k}',\mathbf{k}) \left[f_0' + (1-f_0')\exp\left(\frac{\varepsilon-\varepsilon'}{k_B T}\right)\right]. \tag{6}$$

Moreover, $\tau(\mathbf{k})$ is averaged on the same energy state ε with

$$\frac{1}{\tau(\varepsilon)} = \frac{1}{D(\varepsilon)} \sum_{\mathbf{k}} \frac{1}{\tau(\mathbf{k})} \delta(\varepsilon - \varepsilon_{\mathbf{k}}), \tag{7}$$

where $D(\varepsilon)$ is density of state per unit volume. The RTA collision term is rigorously derived from the full collision

term with only three assumptions: weak deviation from equilibrium, equilibrium phonon distribution, and isotropic electron-phonon scattering. The former two assumptions are widely adopted for investigation of transport and the last assumption of isotropic scattering is nearly valid at temperature higher than Debye temperature. Thus, the Pauli exclusion principle is automatically satisfied in the RTA model, which represents a good approximation of original collision term.

The remaining problem is to solve the transition rate $S(\mathbf{k}', \mathbf{k})$ in Eqs. (6) and (7). Given by Fermi's golden rule, the transition rate is formulated as [32]

$$S(\mathbf{k}', \mathbf{k}) = \sum_{\gamma} \frac{2\pi}{\hbar} |g(\mathbf{k}', \mathbf{k}, \gamma)|^2 \{n(\mathbf{q}, \gamma)\delta(\varepsilon_{\mathbf{k}'} + \hbar\omega_{\mathbf{q},\gamma} - \varepsilon_{\mathbf{k}})\delta_{\mathbf{G},\mathbf{k}'+\mathbf{q}-\mathbf{k}} + [n(-\mathbf{q}, \gamma) + 1]\delta(\varepsilon_{\mathbf{k}'} - \hbar\omega_{-\mathbf{q},\gamma} - \varepsilon_{\mathbf{k}})\delta_{\mathbf{G},\mathbf{k}'+\mathbf{q}-\mathbf{k}}\}, \quad (8)$$

where $\mathbf{q}, \gamma$ is wave vector and polarization of phonon, respectively, and $\mathbf{G}$ is the reciprocal lattice vector. $n(\mathbf{q}, \gamma)$ is the average phonon occupation number and here is denoted by Bose-Einstein distribution under the assumption of local equilibrium state. $g(\mathbf{k}', \mathbf{k}, \gamma)$ is termed as the coupling function representing the strength of electron-phonon scattering. $n(\mathbf{q}, \gamma) = n(-\mathbf{q}, \gamma)$ and $\omega_{\mathbf{q},\gamma} = \omega_{-\mathbf{q},\gamma}$ are used as a result of translational symmetry of the crystal lattice. With the help of the property of the Dirac δ function: $\int \delta(\varepsilon' - \varepsilon_{\mathbf{k}'})d\varepsilon' = 1$ and $\int \delta(\omega - \omega_{\mathbf{q},\gamma})d\omega = 1$, the following dimensionless quantity is introduced as [33,34]:

$$C_{\mathrm{ep}}(\varepsilon, \varepsilon', \omega, \gamma) = \frac{1}{\hbar D(\varepsilon)} \sum_{\mathbf{k},\mathbf{k}'} |g(\mathbf{k}', \mathbf{k}, \gamma)|^2 \delta(\varepsilon' - \varepsilon_{\mathbf{k}'})\delta(\omega - \omega_{\mathbf{q},\gamma})\delta(\varepsilon - \varepsilon_{\mathbf{k}})\delta_{\mathbf{G},\mathbf{k}'+\mathbf{q}-\mathbf{k}}. \quad (9)$$

For the convenience of considering the deviation of single-particle energy from the Fermi energy, the Eliashberg function is introduced and related to the quantity in Eq. (9) as $\alpha^2F(\omega, \gamma) \simeq \sqrt{\varepsilon/\varepsilon_{\mathrm{F}}}C_{\mathrm{ep}}(\varepsilon, \varepsilon', \omega, \gamma)$ [34]. In this way, the scattering rate Eq. (7) is formulated as

$$\frac{1}{\tau(\varepsilon)} = 2\pi\sqrt{\frac{\varepsilon_{\mathrm{F}}}{\varepsilon}} \sum_{\gamma} \int d\omega\alpha^2F(\omega, \gamma)\left\{n(\omega)\left[f_0(\varepsilon - \hbar\omega) + [1 - f_0(\varepsilon - \hbar\omega)]\exp\left(\frac{\hbar\omega}{k_{\mathrm{B}}T}\right)\right]\right.$$
$$\left. + [n(\omega) + 1]\left[f_0(\varepsilon + \hbar\omega) + [1 - f_0(\varepsilon + \hbar\omega)]\exp\left(\frac{-\hbar\omega}{k_{\mathrm{B}}T}\right)\right]\right\}. \quad (10)$$

The Eliashberg function characterizing the strength of electron-phonon coupling can be determined from *ab initio* theoretical calculation [35] or experimental measurement [32]. An empirical expression originally derived in the low-frequency limit is often adopted for the Eliashberg function in the whole frequency spectrum: $\alpha^2F(\omega) = \lambda n(\omega/\omega_D)^n/2$ [36], with n equal to 2 for a clean bulk crystal. λ is the mass enhancement parameter, which can be inversely determined once the Eliashberg function is obtained: $\lambda = 2\int_0^{\omega_{\max}} \frac{\alpha^2F(\omega)}{\omega}d\omega$. The average temperature of the system is adopted for the temperature in Eq. (10), as a tiny temperature difference is considered throughout the system, whereas the local temperature is adopted for the temperature in the local equilibrium distribution of the collision term. Then, the BTE under RTA without magnetic field for electron transport is finally obtained as

$$\frac{\partial f}{\partial t} + \mathbf{v} \cdot \nabla_{\mathbf{r}} f - \frac{e\mathbf{E}}{\hbar} \cdot \nabla_{\mathbf{k}} f = -\frac{f - f_0}{\tau}, \quad (11)$$

where the relaxation time τ is given by Eq. (10).

In principle, there exists an induced electrical field by the drift of electrons under the temperature gradient, which is known as the thermoelectric effect described by the Seebeck coefficient. Nevertheless, the effect on electron thermal transport from the induced electrical field is negligibly small as compared to that from the temperature gradient [37,38]. For steady-state in-plane thermal transport through metal thin film, the inner electric field induced by the temperature gradient can be analytically calculated and its contribution to the electronic thermal conductivity is found to be generally less than 0.03% even for the film thickness up to bulk limit. For steady-state cross-plane thermal transport through metal thin film, it is not feasible to obtain an analytical solution of the electron BTE. Later we will numerically calculate the diffusive current induced by thermal transport when ignoring the inner electric field. The diffusive current can be treated as the effect from an effective electric field, the heat flux carried by which is found to be still negligible compared to the total heat flux.

2. *Deviational formulation*

The response of electrons in metal to the electric field is different from that to the thermal field. The electrons will drift as a whole in the wave vector space under the electric field, whereas only electrons around the Fermi level with a width about the unit thermal energy ($k_{\mathrm{B}}T$) will respond to thermal perturbation [10]. Therefore, one has to track the distribution function in the entire wave vector space in Eq. (11) by the Monte Carlo scheme for electrical transport. For thermal transport, it is not necessary and even not feasible to track the distribution function in the entire wave vector space. Thus we propose to consider the occupied states above the Fermi energy (corresponding to the distribution function f) and the unoccupied states below the Fermi energy [corresponding to (1-f)] in the numerical simulation of electron thermal transport [39]. Furthermore, we introduce the deviational formulation in the variance reduction method to reduce both

the statistical uncertainty and the computational burden [27]. Below we will demonstrate the statistical definition of the macroscopic field variables that can be reformulated into a very elegant form in terms of the deviational scheme.

The excitation energy density is defined as the difference between total internal energy density of electron system and total internal energy density at ground state [40]:

$$\begin{aligned}\Delta U &= U(T) - U(0) \\ &= \int_{4\pi}\int_0^{\infty} \varepsilon f \frac{D(\varepsilon)}{4\pi} d\varepsilon d\mathbf{\Omega} - \int_0^{\varepsilon_F} \varepsilon D(\varepsilon) d\varepsilon, \end{aligned} \tag{12}$$

where $\mathbf{\Omega}$ denotes the solid angle. With the help of electron number conservation from ground state to excitation state, Eq. (12) is rewritten into

$$\begin{aligned}\Delta U = &\int_{4\pi}\int_0^{\varepsilon_F} (\varepsilon_F - \varepsilon)(1-f)\frac{D(\varepsilon)}{4\pi} d\varepsilon d\mathbf{\Omega} \\ &+ \int_{4\pi}\int_{\varepsilon_F}^{\infty} (\varepsilon - \varepsilon_F) f \frac{D(\varepsilon)}{4\pi} d\varepsilon d\mathbf{\Omega}. \end{aligned} \tag{13}$$

We introduce the deviational formulation, and the deviational excitation energy density is obtained as

$$\begin{aligned}\Delta U - \Delta U_{eq} = &\int_{4\pi}\int_0^{\varepsilon_F} (\varepsilon_F - \varepsilon)(-(f - f_{eq}))\frac{D(\varepsilon)}{4\pi} d\varepsilon d\mathbf{\Omega} \\ &+ \int_{4\pi}\int_{\varepsilon_F}^{\infty} (\varepsilon - \varepsilon_F)(f - f_{eq}) \frac{D(\varepsilon)}{4\pi} d\varepsilon d\mathbf{\Omega}, \end{aligned} \tag{14}$$

where f_{eq} is the referenced Fermi-Dirac equilibrium distribution at the temperature T_{eq}. The local temperature is determined by assuming the deviational excitation energy density Eq. (14) to be equal to that at an equivalent equilibrium temperature T_{loc}:

$$\begin{aligned}\Delta U - \Delta U_{eq} = &\int_0^{\varepsilon_F} (\varepsilon_F - \varepsilon)[-(f_0(T_{loc}) - f_{eq})] D(\varepsilon) d\varepsilon \\ &+ \int_{\varepsilon_F}^{\infty} (\varepsilon - \varepsilon_F)(f_0(T_{loc}) - f_{eq}) D(\varepsilon) d\varepsilon. \end{aligned} \tag{15}$$

The statistical definition of overall heat flux in the electron system is expressed as [10]

$$\mathbf{q} = \int_{4\pi}\int_0^{\infty} \mathbf{v_k}(\varepsilon - \mu) f \frac{D(\varepsilon)}{4\pi} d\varepsilon d\mathbf{\Omega}. \tag{16}$$

The scope of integration over the energy level in Eq. (16) is separated into a section below the Fermi level and a section above the Fermi level:

$$\begin{aligned}\mathbf{q} = &\int_{4\pi}\int_0^{\mu} \mathbf{v_k}(\mu - \varepsilon)(1-f)\frac{D(\varepsilon)}{4\pi} d\varepsilon d\mathbf{\Omega} \\ &+ \int_{4\pi}\int_{\mu}^{\infty} \mathbf{v_k}(\varepsilon - \mu) f \frac{D(\varepsilon)}{4\pi} d\varepsilon d\mathbf{\Omega}. \end{aligned} \tag{17}$$

We introduce further the deviational description, and the heat flux expression in Eq. (17) becomes

$$\begin{aligned}\mathbf{q} = &\int_{4\pi}\int_0^{\mu} \mathbf{v_k}(\mu - \varepsilon)(-(f - f_{eq}))\frac{D(\varepsilon)}{4\pi} d\varepsilon d\mathbf{\Omega} \\ &+ \int_{4\pi}\int_{\mu}^{\infty} \mathbf{v_k}(\varepsilon - \mu)(f - f_{eq}) \frac{D(\varepsilon)}{4\pi} d\varepsilon d\mathbf{\Omega}. \end{aligned} \tag{18}$$

The statistical definition of electric current is expressed as

$$\mathbf{J} = -e\int_{4\pi}\int_0^{\infty} \mathbf{v_k} f \frac{D(\varepsilon)}{4\pi} d\varepsilon d\mathbf{\Omega}, \tag{19}$$

which can be reformulated into the deviational description as

$$\mathbf{J} = -e\int_{4\pi}\int_0^{\infty} \mathbf{v_k}(f - f_{eq}) \frac{D(\varepsilon)}{4\pi} d\varepsilon\, d\mathbf{\Omega}. \tag{20}$$

In the electron heat transport, when neglecting the induced inner electric field, the heat flux carried by the diffusive current is computed as

$$\begin{aligned}\mathbf{q}_{diff} = &\int_{4\pi}\int_{\mu}^{\infty} \mathbf{v_k}(\varepsilon - \mu)(f - f_{eq})\frac{D(\varepsilon)}{4\pi} d\varepsilon d\mathbf{\Omega} \\ &- \int_{4\pi}\int_0^{\mu} \mathbf{v_k}(\mu - \varepsilon)(-(f - f_{eq}))\frac{D(\varepsilon)}{4\pi} d\varepsilon d\mathbf{\Omega}, \end{aligned} \tag{21}$$

which is considerably smaller compared to Eq. (18).

For a compact mathematical expression for electron thermal transport, we introduce the following deviational distribution function:

$$g^d = [1 - 2H(\mu - \varepsilon)](f - f_{eq}), \tag{22}$$

where $H(\mu - \varepsilon)$ is the Heaviside step function. The electron BTE for thermal transport is reformulated as

$$\frac{\partial g^d}{\partial t} + \mathbf{v}\cdot\nabla_{\mathbf{r}} g^d = -\frac{g^d - g^d_{loc}}{\tau}, \tag{23}$$

where $g^d_{loc} = \{\exp(|\varepsilon - \mu|/k_B T_{loc}) + 1\}^{-1} - \{\exp(|\varepsilon - \mu|/k_B T_{eq}) + 1\}^{-1}$ is the local deviational equilibrium distribution with T_{loc} determined by Eq. (15). If $T > T_{eq}$, the sign of deviational distribution function g^d is positive; otherwise, the sign is negative. In this way, the deviational excitation energy density Eq. (14), the overall heat flux Eq. (18) and the heat flux carried by the diffusive current Eq. (21) are reformulated into

$$\Delta U - \Delta U_{eq} = \int_{4\pi}\int_0^{\infty} |\varepsilon - \varepsilon_F| g^d \frac{D(\varepsilon)}{4\pi} d\varepsilon d\mathbf{\Omega}, \tag{24}$$

$$\mathbf{q} = \int_{4\pi}\int_0^{\infty} \mathbf{v_k}|\varepsilon - \mu| g^d \frac{D(\varepsilon)}{4\pi} d\varepsilon d\mathbf{\Omega}, \tag{25}$$

$$\mathbf{q}_{diff} = \int_{4\pi}\int_0^{\infty} \mathbf{v_k}(\varepsilon - \mu) g^d \frac{D(\varepsilon)}{4\pi} d\varepsilon d\mathbf{\Omega}. \tag{26}$$

For electrical transport, the deviational formulation is slightly different from that for thermal transport as inferred from Eq. (20). The deviational distribution is introduced as $g^d = f - f_{eq}$ in the entire wave vector space. The electron BTE for charge transport is reformulated as

$$\frac{\partial g^d}{\partial t} + \mathbf{v}\cdot\nabla_{\mathbf{r}} g^d - \frac{e\mathbf{E}}{\hbar}\cdot\nabla_{\mathbf{k}} g^d = -\frac{g^d - g^d_{loc}}{\tau} + \frac{e\mathbf{E}}{\hbar}\cdot\nabla_{\mathbf{k}} f_{eq}, \tag{27}$$

where the deviational equilibrium distribution is $g^d_{loc} = f_0(T_{loc}) - f_{eq}$, and the extra source term comes from the drift

in wave vector space as a whole. The sign of deviational distribution function g^d is different from that for thermal transport because the temperature stays nearly unchanged in electrical transport. If g^d is larger than zero with excess electrons, the deviational sign is positive, and otherwise negative. The statistical definition of the electric current Eq. (20) is thus reformulated into

$$\mathbf{J} = -e \int_{4\pi} \int_0^{\infty} \mathbf{v}_{\mathbf{k}} g^d \frac{D(\varepsilon)}{4\pi} d\varepsilon d\mathbf{\Omega}. \tag{28}$$

B. Monte Carlo algorithm

In this subsection, we will introduce the Monte Carlo algorithm to solve the electron BTE for thermal and electrical transport in metal nanostructures. In recent decades there has been much progress in Monte Carlo schemes for nanoscale phonon heat transport in semiconductors and insulators [27,41,42]. However, the Monte Carlo scheme for nanoscale electron heat transport in metals remains to be established. Although the BTE [Eq. (23)] for electron heat transport is very similar to the phonon BTE under RTA, there are several essential differences between phonons and electrons: (i) phonons are bosons with Bose-Einstein statistics, whereas electrons are fermions with Fermi-Dirac statistics; (ii) phonons mainly scatter among themselves whereas electrons scatter mainly with lattice vibration (phonons). In addition, although the EMC for electron transport in semiconductors has been well developed, it is difficult to adapt the EMC to electron thermal transport in metals because of their different energy band structures: only the electrons in the conduction band above the Fermi energy level (n-type) or the holes in the valence band below the Fermi energy level (p-type) are tracked in EMC for semiconductors, whereas the electron states both above and below the Fermi energy level shall be carefully tracked in the Monte Carlo scheme for metals. Note that the RTA model has implicitly included the Pauli exclusion principle so that no additional scheme has to be considered for the occupation of final states in the implementation of scattering process compared to EMC in doped semiconductors [43,44]. Below we describe the details of the deviational Monte Carlo schemes for electron thermal transport in Sec. II B 1, which mainly include the following steps: initialization, drift, boundary treatment, macroscopic variable calculation and scattering. The Monte Carlo algorithm is slightly adjusted for electrical transport in Sec. II B 2, with an introduction to the treatment of the equivalent source term in Eq. (27).

1. Thermal transport

(a) Initialization. Deviational particles are used to represent the deviational distribution function defined in Eq. (22) [27]. We choose a referenced equilibrium state at a temperature T_{eq}. For numerical integration, a Fermi window $[\varepsilon_{\text{l}}, \varepsilon_{\text{h}}]$ is taken into account, where the lower limit and upper limit is, respectively, $\varepsilon_{\text{l}} = \varepsilon_{\text{F}} - 10k_{\text{B}}T$ and $\varepsilon_{\text{h}} = \varepsilon_{\text{F}} + 10k_{\text{B}}T$ after an independence check, with T being the system average temperature. If the system is initially at an equilibrium state at a temperature T_0, the initial number of deviational particles is determined as

$$\begin{aligned} N_{\text{ini}} &= \frac{1}{N_{\text{eff}}} \int_{\varepsilon_{\text{l}}}^{\varepsilon_{\text{h}}} |g^d D(\varepsilon)| d\varepsilon \\ &= \frac{1}{N_{\text{eff}}} \int_{\varepsilon_{\text{l}}}^{\varepsilon_{\text{h}}} |[\exp(|\varepsilon - \mu|/k_{\text{B}}T_0) + 1]^{-1} \\ &\quad - [\exp(|\varepsilon - \mu|/k_{\text{B}}T_{\text{eq}}) + 1]^{-1}| D(\varepsilon) d\varepsilon, \end{aligned} \tag{29}$$

with N_{eff} a scaling factor. If $T_0 > T_{\text{eq}}$, the deviational particles are assigned a positive sign, otherwise a negative sign. The position of the deviational particles is uniformly distributed in the simulation domain. The energy level of the deviational particles is drawn from the cumulative integrand function from Eq. (29). Once the energy level is obtained, the magnitude of the particle velocity is determined based on the energy band function. The direction of the particle velocity is uniformly distributed in the solid angle space similar to the treatment in Monte Carlo scheme for phonon transport [41].

(b) Drift. The motion of particle j satisfies

$$\mathbf{r}_j(t + \Delta t) = \mathbf{r}_j(t) + \mathbf{v}_j \Delta t, \tag{30}$$

which drifts linearly with velocity unchanged unless encountering the boundary within the drift step. The drift step is performed for each particle.

(c) Boundary treatment. Several kinds of boundary treatments are introduced including the isothermal boundary, adiabatic boundary, periodic heat flux boundary, and periodic boundary. For the isothermal boundary, the heat bath method originally provided in the phonon Monte Carlo scheme [45] is adapted here, where the particles in the heat bath are assigned instead by the deviational Fermi-Dirac equilibrium distribution at the boundary temperature within each time step. This is in strong contrast to the empirical change of energy state and scaling factor of particles incident on the isothermal boundary in previous work [23–25]. It should be noticed that the length of heat bath shall be larger than the maximum moving distance of one particle within each time step. The fully diffuse scheme is implemented for the adiabatic boundary. The periodic heat flux boundary in phonon Monte Carlo scheme [27,46] is also adapted for in-plane thermal transport, and the periodic boundary is used for the simplification of simulation.

(d) Macroscopic variable calculation. First, the computational domain is divided into a series of unit cells with equal volume V_g and index n. The deviational excitation energy density is computed as

$$(\Delta U - \Delta U_{\text{eq}})_n = \frac{1}{V_g} \sum_{j \in n} |\varepsilon_j - \varepsilon_{\text{F}}| s_d(j), s_d(j) = \pm 1. \tag{31}$$

Thus the local temperature T_n at the n^{th} unit cell is determined by the following inverse numerical integration using the dichotomy method:

$$\begin{aligned} (\Delta U - \Delta U_{\text{eq}})_n = \int_{\varepsilon_{\text{l}}}^{\varepsilon_{\text{h}}} |\varepsilon - \varepsilon_{\text{F}}| \{ &[\exp(|\varepsilon - \mu|/k_{\text{B}}T_n) + 1]^{-1} \\ &- [\exp(|\varepsilon - \mu|/k_{\text{B}}T_{\text{eq}}) + 1]^{-1} \} D(\varepsilon) d\varepsilon. \end{aligned} \tag{32}$$

The overall heat flux for n^{th} unit cell is calculated by

$$\mathbf{q}_n = \frac{1}{V_g}\sum_{j\in n}\mathbf{v}_j|\varepsilon_j-\mu|s_d(j), \tag{33}$$

whereas the heat flux carried by the diffusive current is calculated by

$$\mathbf{q}_{\text{diff},n} = \frac{1}{V_g}\sum_{j\in n}\mathbf{v}_j(\varepsilon_j-\mu)s_d(j). \tag{34}$$

(e) Scattering. Scattering is the key step to restoring the electrons to equilibrium state. After each time step, the scattering probability of each particle is determined by the formula $p = 1-\exp(-\Delta t/\tau)$ based on the RTA. The implementation of the scattering step is well established in the deviational Monte Carlo scheme for phonon transport [27] and is adapted here. We randomly delete from the collection of the scattered particles $N^+_{s,n}+N^-_{s,n}-|N^+_{s,n}-N^-_{s,n}|$ with $N^+_{s,n}$ being the scattered deviational particle with positive sign and $N^-_{s,n}$ is the scattered deviational particle with negative sign in the n^{th} unit cell. The properties of the remaining $|N^+_{s,n}-N^-_{s,n}|$ particles are redrawn from the following distribution:

$$g^d_{\text{loc}}\frac{D(\varepsilon)}{\tau(\varepsilon)} = \{[\exp(|\varepsilon-\mu|/k_{\text{B}}T_{\text{loc}})+1]^{-1} - [\exp(|\varepsilon-\mu|/k_{\text{B}}T_{\text{eq}})+1]^{-1}\}\frac{D(\varepsilon)}{\tau(\varepsilon)}, \tag{35}$$

where the local equilibrium distribution is supposed to be at the local temperature in the present work and the deviational sign is given by the sign of g^d_{loc}.

2. Electrical transport

For electrical transport, the deviational particles represent the deviational distribution function defined in Eq. (27). Due to the negligible influence of the electrothermal effect, the system is assumed to keep at a uniform temperature T_0. We choose the referenced equilibrium distribution at the temperature $T_{\text{eq}} = T_0$ with no particles in the initial step.

The particles will be accelerated as $\mathbf{r}_j(t+\Delta t) = \mathbf{r}_j(t) + \mathbf{v}_j\Delta t - \frac{1}{2}\frac{e\mathbf{E}}{m}(\Delta t)^2$ in the drift step where the external electric field is assumed constant in the simulation domain. Note that the electric field should be moderate, which is neither too small to be neglected without numerical error nor too strong to make particles exceed the boundary of the first Brillouin zone. Besides the periodic boundary and the diffuse boundary, the periodic electric current boundary is adopted for in-plane electrical transport where the particles leaving the domain will re-enter from the opposite side to ensure the conservation of electric current.

With the split scheme in the Monte Carlo method, we need to consider the extra source term in Eq. (27) as $\frac{\partial g^d}{\partial t} = \frac{e\mathbf{E}}{\hbar}\cdot\nabla_{\mathbf{k}}f_{\text{eq}}$ additionally for electrical transport. The number of deviational particles generated by this source term within each time step is computed as

$$\begin{aligned} N_{\text{source}} &= \int_{4\pi}\int_{\varepsilon_{\text{l}}}^{\varepsilon_{\text{h}}}\left|\frac{e\mathbf{E}}{\hbar}\cdot\nabla_{\mathbf{k}}f_{\text{eq}}\right|\frac{D(\varepsilon)}{4\pi}d\varepsilon d\mathbf{\Omega}\Delta t \\ &= \frac{eE\Delta t}{2}\int_{\varepsilon_{\text{l}}}^{\varepsilon_{\text{h}}}\int_0^{\pi} v|\cos\theta\sin\theta\nabla_{\varepsilon}f_{\text{eq}}|D(\varepsilon)d\theta d\varepsilon \\ &= \frac{eE\Delta t}{2}\int_{\varepsilon_{\text{l}}}^{\varepsilon_{\text{h}}} v|\nabla_{\varepsilon}f_{\text{eq}}|D(\varepsilon)d\varepsilon \end{aligned} \tag{36}$$

with $\nabla_{\varepsilon}f_{\text{eq}} = -f_{\text{eq}}(1-f_{\text{eq}})/k_{\text{B}}T_{\text{eq}}$, E being the magnitude of the external electric field. The energy level of particles is drawn from the cumulative integrand function from Eq. (36) whereas the direction of the particle velocity is determined from

$$\begin{aligned} v_{1,j} &= v_j\cos\theta = \begin{cases} v_j\sqrt{R_1}, & \theta\in[0,\pi/2] \\ -v_j\sqrt{R_1}, & \theta\in[\pi/2,\pi] \end{cases}, \\ v_{2,j} &= v_j\sin\theta\sin\varphi = v_j\sqrt{1-R_1}\sin(2\pi R_2), \\ v_{3,j} &= v_j\sin\theta\cos\varphi = v_j\sqrt{1-R_1}\cos(2\pi R_2), \end{aligned} \tag{37}$$

where the subscripts 1, 2, 3 denote the x, y, and z directions separately within the assumption of external electric field along the x direction, and two random numbers are generated as $R_1\in[0,1]$ and $R_2\in[0,1]$. In addition, the deviational particles with $\theta\in[0,\pi/2]$ are assigned a negative sign, whereas the deviational particles with $\theta\in[\pi/2,\pi]$ are assigned a positive sign. The electric current in a unit cell of the simulation domain is calculated as

$$\mathbf{J}_n = -\frac{1}{V_g}\sum_{j\in n}e\mathbf{v}_j s_d(j), \qquad s_d(j) = \pm 1. \tag{38}$$

In the scattering step, the selected scattered particles are directly deleted from the domain due to the choice of $T_{\text{eq}} = T_0$.

III. RESULTS AND DISCUSSION

In this section, the Monte Carlo algorithm developed for thermal and electrical transport in Sec. II B is validated by modeling the in-plane thermal and electrical transport, and the cross-plane thermal transport through a gold thin film around room temperature by comparing to analytical solutions or discrete ordinates solution [20]. The schematics of cross-plane and in-plane electron transport are shown in Fig. 1. The physical parameters of gold at 300 K used in the simulation are given in Table I.

The relaxation time is calculated based on Eq. (10), where the mass enhancement parameter λ in the Eliashberg function is 0.17 from first principle calculations [35] and lies in the range of [0.14, 0.18] from point-contact and femtosecond experimental measurement [32,47,48]. Further, we neglect the dependency of the integrand function on electron energy states close to the Fermi energy in Eq. (10). Then the thermal conductivity of bulk material is calculated by $\kappa_e = \int_0^{\infty}(\varepsilon-\varepsilon_{\text{F}})\frac{df_0}{dT}v^2\tau(\varepsilon)D(\varepsilon)d\varepsilon/3$, which gives the value between 359 and 279 W/m/K for λ from 0.14 to 0.18. This is in acceptable agreement with the experimental bulk value of 317 W/m/K. Below we adopt λ equal to 0.15 with the expression of relaxation time simplified into $\tau(\varepsilon)\simeq\tau_0\sqrt{\varepsilon/\varepsilon_{\text{F}}} = 2.77\times10^{-14}\sqrt{\varepsilon/\varepsilon_{\text{F}}}$ (s).

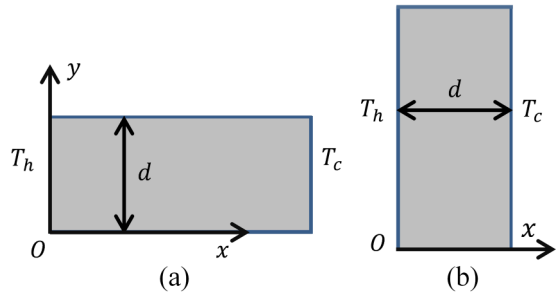

FIG. 1. Schematic of in-plane and cross-plane electron transport through metallic thin film: (a) in-plane transport, the x direction is the periodic heat flux boundary or periodic electric current boundary, the y direction is the adiabatic boundary, and the z direction is the periodic boundary; (b) cross-plane transport, the x direction is the isothermal boundary, the other directions are periodic boundaries.

The average electron MFP is calculated by $\Lambda = \int_0^\infty (\varepsilon - \varepsilon_F)\frac{df_0}{dT} v^2 \tau(\varepsilon) D(\varepsilon) d\varepsilon / \int_0^\infty (\varepsilon - \varepsilon_F)\frac{df_0}{dT} v D(\varepsilon) d\varepsilon$, which produces results in good agreement with the referenced *ab initio* data [49] as shown in Table I. The Knudsen number is defined as $Kn = \Lambda/d$ with d the characteristic length of metallic structure.

In addition to the relaxation time, the energy band structure is also an important parameter for metallic material. For a weakly correlated electron system in the metals studied in this work, the nearly free electron model is a good approximation [10]. Besides, the external electric field is treated as a perturbation such that electrons do not exceed the boundary of the first Brillouin zone to a higher energy band. Thus we adopt a parabolic energy band function as $\varepsilon = \hbar^2\mathbf{k}^2/2m = m\mathbf{v}^2/2$ inside the first Brillouin zone with m being the mass of the electron. A more realistic and accurate band structure could be, in principle, obtained by the *ab initio* method [50] and incorporated into the present numerical framework in a straightforward way.

A. In-plane electron thermal transport

In this subsection and below, the in-plane and cross-plane thermal transport at nanoscale where the Fourier's law is invalid are simulated. First, we consider the in-plane electron thermal transport through a gold thin film with a thickness from 2 to 400 nm as shown in Fig. 1(a). The time step in the simulation is chosen from $\tau_0/200$ to $\tau_0/40$ with increasing film thickness. The scaling factor is set to be 5 for all the cases. The periodic heat flux boundary condition is implemented along the x direction with a length of 200 nm and the temperature difference of 20 K, whereas the periodic boundary condition is used for the z direction with a width chosen such that the number of computational particles varies around 10^5. After the simulation reaches the steady state, the results within 2000 time steps are sampled every 10 time steps for the time averaging of macroscopic variables. Figure 2 shows the cross-section overall heat flux distribution without subtracting the heat flux carried by the diffusive current and the effective thermal conductivity obtained by the present Monte Carlo simulation in comparison to the analytical solution of the classical F-S model [13,14]. The current Monte Carlo scheme captures well the general profile of cross-section heat flux distribution and provides a good prediction of the effective thermal conductivity in spite of existing fluctuations due to the stochastic nature of the method. Similar to the result of in-plane phonon heat transport [51], the heat flux near the boundary will be reduced due to the enhancement of electron-boundary scattering with the decrease of film thickness. Thus

TABLE I. Physical parameters of bulk gold at $T = 300$ K.

Parameter	ε_F/eV	Θ_D/K	λ	Λ/nm(present)	Λ/nm[49]
Value	5.51	165	0.15	38.6	37.7

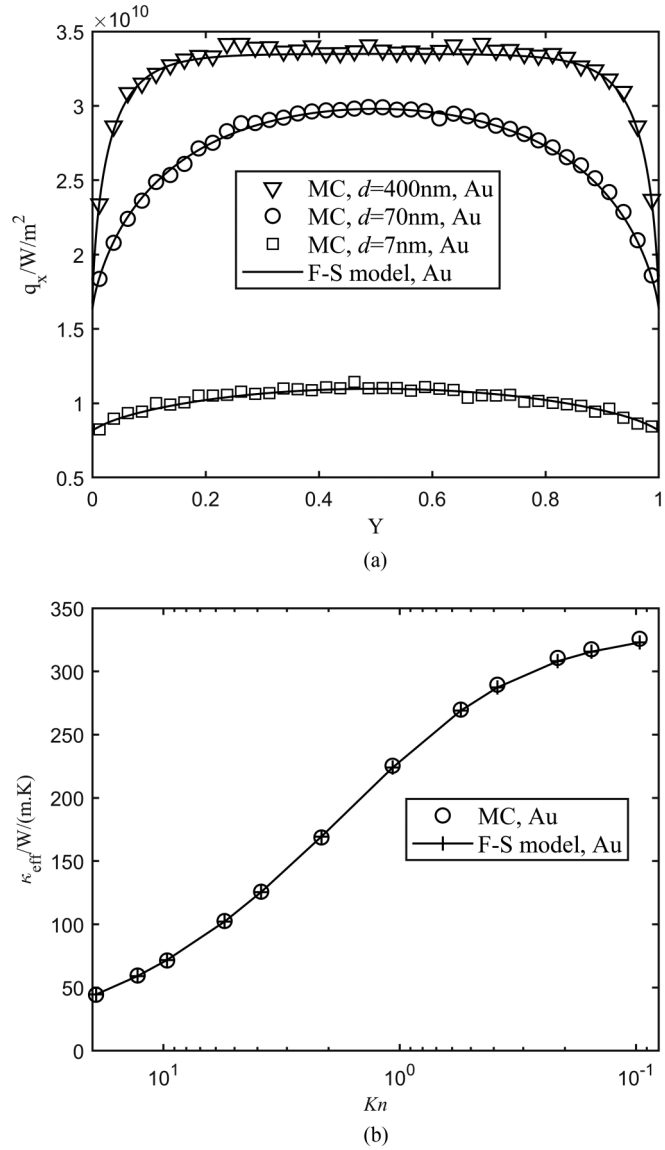

FIG. 2. The cross-section overall heat flux distribution and effective thermal conductivity of in-plane transport through an Au thin film: (a) cross-section heat flux distribution with thickness of 7, 70, and 400 nm, respectively. Symbols are the results from the present Monte Carlo scheme whereas solid lines are that of the F-S model [13,14]; (b) effective thermal conductivity versus Knudsen number.

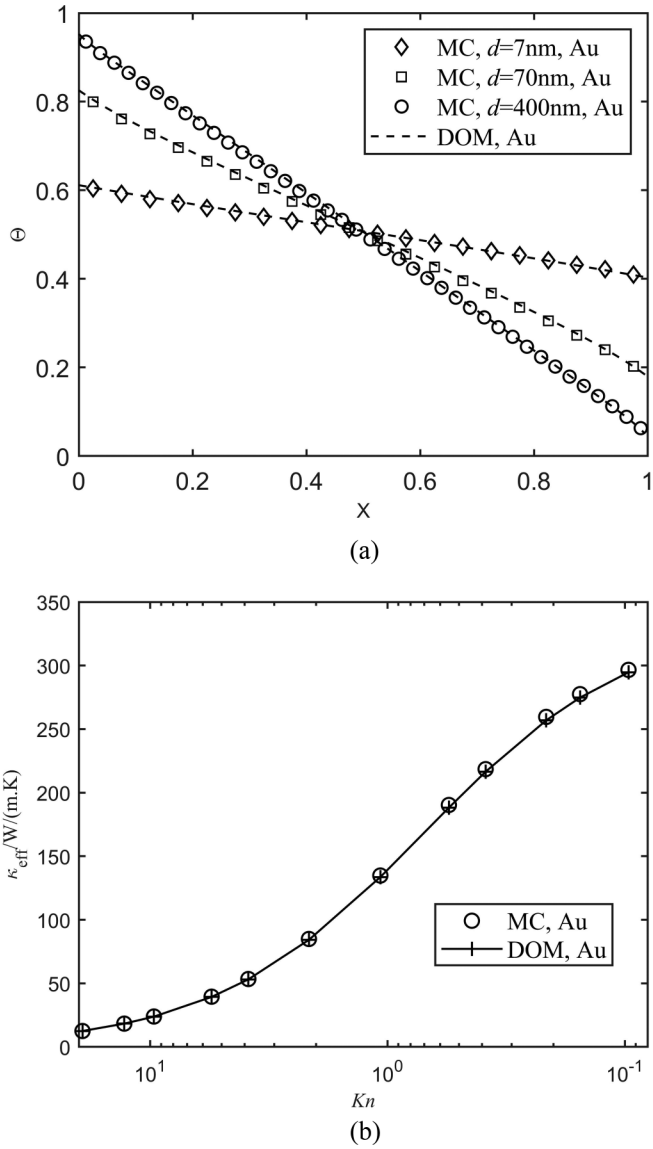

FIG. 3. The nondimensional temperature distribution and effective thermal conductivity of cross-plane transport through the Au thin film at steady state: (a) nondimensional temperature distribution with thickness of 7, 70, and 400 nm, respectively. Symbols are the results from the present Monte Carlo scheme, whereas dashed lines are that of discrete ordinates method; (b) effective thermal conductivity versus Knudsen number.

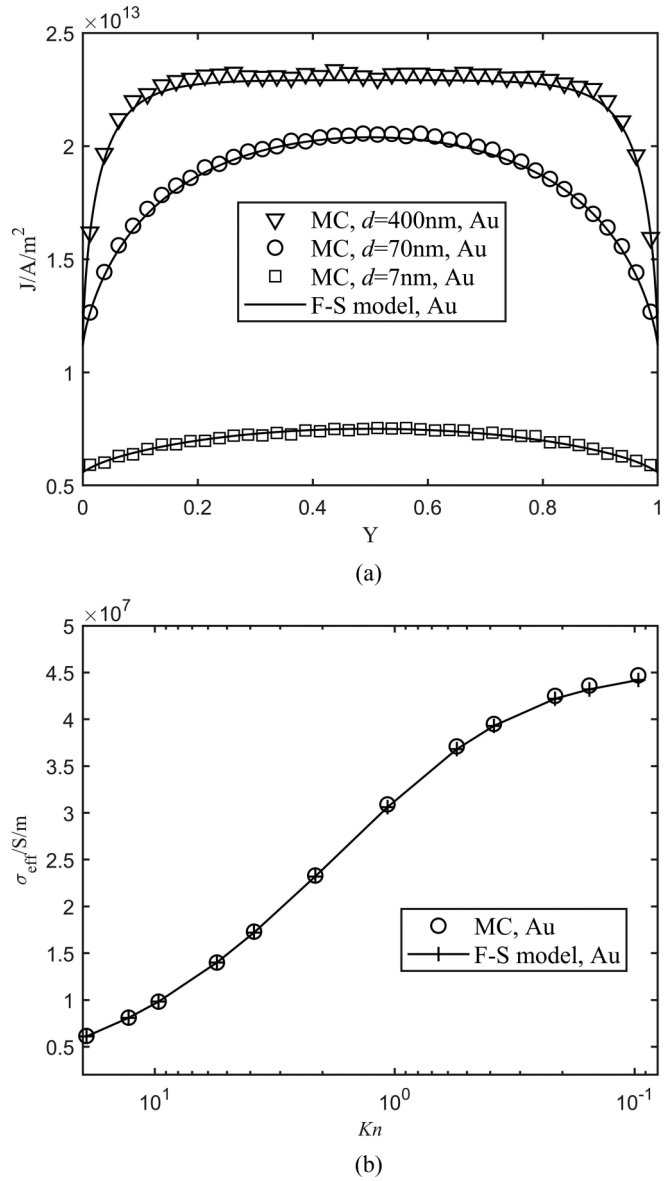

FIG. 4. The cross-section electric current distribution and effective electrical conductivity of in-plane transport through the Au thin film: (a) cross-section electric current distribution with thickness of 7, 70, and 400 nm, respectively. Symbols are the results from the present Monte Carlo scheme, whereas solid lines are that of the F-S model [13]; (b) effective electrical conductivity versus Knudsen number.

the heat flux profile becomes no longer uniform as predicted by Fourier's law. With infinitely decreasing film thickness, the heat flux profile approaches to be nearly uniform again in the ballistic transport regime where electron-boundary scattering is dominant.

B. Cross-plane electron thermal transport

Then we consider the cross-plane electron thermal transport through gold thin film with a thickness from 2 to 400 nm as shown in Fig. 1(b). The left-hand and right-hand sides of the thin film keep in contact with a hot source at 310 K and a cold source at 290 K, respectively. The time step is chosen from $\tau_0/200$ to $\tau_0/40$ with increasing film thickness. The scaling factor is equal to 5 for all the cases. The periodic boundary condition is applied for both y and z directions with a side size chosen such that the number of computational particles varies around 10^5. When the simulation reaches the steady state, the results within 1000 time steps are sampled every 10 time steps for the time averaging of macroscopic variables. As the analytical solution of cross-plane transport is not available, we use our homemade discrete ordinates solution as the benchmark. The validity of our discrete ordinates method has been demonstrated in our previous work [20,52]. The comparison between the results

from our current Monte Carlo scheme and those from the discrete ordinates method is shown in Fig. 3. The temperature distribution within thin film is linear, with a temperature jump at the boundary increasing as the film thickness decreases. This boundary temperature jump comes from the in-sufficient thermalization between the heat bath and thin film. Thus the effective cross-plane thermal conductivity calculated from the overall heat flux decreases with decreasing thin film thickness. Besides, the thermal conductivity contributed by the diffusive current lies in the range of [0.2, 9] (W/m/K) for all the film thicknesses considered in the present work, the proportion of which in the overall thermal conductivity decreases when increasing thickness and is generally less than 5%. Note that this diffusive current corresponds to an effective induced electric field, the neglecting of which is thus applicable. The excellent agreement of the results by the present Monte Carlo scheme with that by the discrete ordinates method for cross-plane electron thermal transport further validates our algorithm.

C. In-plane electrical transport

In order to validate the Monte Carlo treatment of electrical transport, we consider only the in-plane case with the number of simulating particles nearly half of that in the corresponding in-plane thermal transport case. The periodic electric current boundary is adopted with the electric field equal to 5×10^5 V/m. The excellent agreement of the current Monte Carlo treatment with the F-S model for electrical transport validates our MC algorithm, as is shown in Fig. 4.

IV. CONCLUSIONS

Through transforming the full collision term in the electron Boltzmann equation into the relaxation time approximation form, a deviational Monte Carlo algorithm is developed for thermal and electrical transport in metallic nanostructures. We propose to track the occupied electron states above the Fermi energy level and the unoccupied electron states below the Fermi energy level for an efficient simulation of electron thermal transport. An additional equivalent source term is implemented for electrical transport due to the drift of electrons in the wave vector space as a whole in contrast to thermal transport. The present Monte Carlo scheme is extensively validated by modeling in-plane and cross-plane thermal transport, as well as in-plane electrical transport through metallic thin films. Thermal and electrical transport in more complex geometries such as the nanocrystalline and nanoporous metallic structures will be explored in future work. Besides, more realistic, accurate band structure can be incorporated into the present numerical framework in a straightforward way in the near future. This work will provide a fundamental understanding of electron transport in micro- and nanoscale, and a ground for the study of electron-phonon coupling transport.

ACKNOWLEDGMENTS

This work was financially supported by a National Science Foundation (NSF) grant of China (Grants No. 51621062 and No. 91634107) and Tsinghua University Initiative Scientific Research Program. We appreciate the anonymous reviewers for their valuable comments.

[1] K. S. Novoselov, V. Fal, L. Colombo, P. Gellert, M. Schwab, and K. Kim, A roadmap for graphene, Nature (London) **490**, 192 (2012).

[2] A. A. Balandin, Thermal properties of graphene and nanostructured carbon materials, Nat. Mater. **10**, 569 (2011).

[3] A. M. Marconnet, M. A. Panzer, and K. E. Goodson, Thermal conduction phenomena in carbon nanotubes and related nanostructured materials, Rev. Mod. Phys. **85**, 1295 (2013).

[4] J. A. Davis, R. Venkatesan, A. Kaloyeros, M. Beylansky, S. J. Souri, K. Banerjee, K. C. Saraswat, A. Rahman, R. Reif, and J. D. Meindl, Interconnect limits on gigascale integration (GSI) in the 21st century, Proc. IEEE **89**, 305 (2001).

[5] D. Grimm, R. B. Wilson, B. Teshome, S. Gorantla, M. H. Rummeli, T. Bublat, E. Zallo, G. Li, D. G. Cahill, and O. G. Schmidt, Thermal conductivity of mechanically joined semiconducting/metal nanomembrane superlattices, Nano Lett. **14**, 2387 (2014).

[6] M. Mikulics, P. Kordoš, A. Fox, M. Kočan, H. Lüth, Z. Sofer, and H. Hardtdegen, Efficient heat dissipation in AlGaN/GaN heterostructure grown on silver substrate, Appl. Mater. Today **7**, 134 (2017).

[7] Y. Wang, Z. Lu, and X. Ruan, First principles calculation of lattice thermal conductivity of metals considering phonon-phonon and phonon-electron scattering, J. Appl. Phys. **119**, 225109 (2016).

[8] A. Jain and A. J. H. McGaughey, Thermal transport by phonons and electrons in aluminum, silver, and gold from first principles, Phys. Rev. B **93**, 081206(R) (2016).

[9] S.-Y. Yue, X. Zhang, S. Stackhouse, G. Qin, E. Di Napoli, and M. Hu, Methodology for determining the electronic thermal conductivity of metals via direct nonequilibrium *ab initio* molecular dynamics, Phys. Rev. B **94**, 075149 (2016).

[10] Ziman, *Electrons and phonons: The Theory of Transport Phenomena in Solids* (Clarendon, Oxford, 1960).

[11] B. Feng, Z. Li, and X. Zhang, Prediction of size effect on thermal conductivity of nanoscale metallic films, Thin Solid Films, **517**, 2803 (2009).

[12] M. Flik and C. Tien, Size effect on the thermal conductivity of high-T_c thin-film superconductors, J. Heat Transfer **112**, 872 (1990).

[13] K. Fuchs and N. F. Mott, The conductivity of thin metallic films according to the electron theory of metals, Math. Proc. Camb. Philos. Soc. **34**, 100 (1938).

[14] E. H. Sondheimer, The mean free path of electrons in metals, Adv. Phys. **1**, 1 (1952).

[15] A. F. Mayadas and M. Shatzkes, Electrical-resistivity model for polycrystalline films: The case of arbitrary reflection at external surfaces, Phys. Rev. B **1**, 1382 (1970).

[16] N. Stojanovic, D. H. S. Maithripala, J. M. Berg, and M. Holtz, Thermal conductivity in metallic nanostructures at high temperature: Electrons, phonons, and the Wiedemann-Franz law, Phys. Rev. B **82**, 075418 (2010).
[17] S. Kumar and G. C. Vradis, Thermal conductivity of thin metallic film, J. Heat Transfer **116**, 28 (1994).
[18] D. Stewart and P. M. Norris, Size effects on the thermal conductivity of thin metallic wires: Microscale implications, Microsc. Therm. Eng. **4**, 89 (2000).
[19] J. S. Jin, J. S. Lee, and O. Kwon, Electron effective mean free path and thermal conductivity predictions of metallic thin films, Appl. Phys. Lett. **92**, 171910 (2008).
[20] Y. Guo and M. Wang, Heat transport in two-dimensional materials by directly solving the phonon Boltzmann equation under Callaway's dual relaxation model, Phys. Rev. B **96**, 134312 (2017).
[21] C. Jacoboni and L. Reggiani, The Monte Carlo method for the solution of charge transport in semiconductors with applications to covalent materials, Rev. Mod. Phys. **55**, 645 (1983).
[22] C. Kittle, *Introduction to Solid State Physics* (Wiley, New York, 2005).
[23] B. T. Wong and M. P. Mengüç, Electronic thermal conduction in thin gold film, in *ASME 2003 Heat Transfer Summer Conference* (ASME, New York, 2003), pp. 715.
[24] B. T. Wong and M. P. Mengüç, *Thermal Transport for Applications in Micro/nanomachining* (Springer, Berlin, 2008).
[25] B. T. Wong and M. Pinar Mengüç, A unified Monte Carlo treatment of the transport of electromagnetic energy, electrons, and phonons in absorbing and scattering media, J. Quant. Spectrosc. Radiat. Trans. **111**, 399 (2010).
[26] L. L. Baker and N. G. Hadjiconstantinou, Variance reduction for Monte Carlo solutions of the Boltzmann equation, Phys. Fluids. **17**, 051703 (2005).
[27] J.-P. M. Péraud and N. G. Hadjiconstantinou, Efficient simulation of multidimensional phonon transport using energy-based variance-reduced Monte Carlo formulations, Phys. Rev. B **84**, 205331 (2011).
[28] M. Kaviany, *Heat Transfer Physics* (Cambridge University Press, New York, 2014).
[29] J. M. Ziman, *Principles of the Theory of Solids*, (Cambridge University Press, Cambridge, 1972).
[30] R. Soto, *Kinetic Theory and Transport Phenomena* (Oxford University Press, Oxford, 2016).
[31] M. Lundstrom, *Fundamentals of Carrier Transport* (Cambridge University Press, Cambridge, 2000).
[32] G. Grimvall, *The Electron-Phonon Interaction in Metals* (North-Holland, New York, 1981).
[33] P. B. Allen, Theory of Thermal Relaxation of Electrons in Metals, Phys. Rev. Lett. **59**, 1460 (1987).
[34] S. Ono, Thermalization in simple metals: Role of electron-phonon and phonon-phonon scattering, Phys. Rev. B **97**, 054310 (2018).
[35] R. Bauer, A. Schmid, P. Pavone, and D. Strauch, Electron-phonon coupling in the metallic elements Al, Au, Na, and Nb: A first-principles study, Phys. Rev. B **57**, 11276 (1998).
[36] V. V. Kabanov and A. S. Alexandrov, Electron relaxation in metals: Theory and exact analytical solutions, Phys. Rev. B **78**, 174514 (2008).
[37] Z. M. Zhang, *Nano/microscale Heat Transfer* (Mc Graw Hill, New York, 2007).
[38] T. M. Tritt, *Thermal conductivity: Theory, Properties, and Applications* (Springer Science & Business Media, New York, 2005).
[39] P. J. v. Hall, Ultrafast processes in Ag and Au: A Monte carlo study, Phys. Rev. B **63**, 104301 (2001).
[40] G. Chen, *Nanoscale Energy Transport and Conversion: A Parallel Treatment of Electrons, Molecules, Phonons, and Photons* (Oxford University Press, New York, 2005).
[41] S. Mazumder and A. Majumdar, Monte Carlo study of phonon transport in solid thin films including dispersion and polarization, J. Heat Transfer **123**, 749 (2001).
[42] R. Peterson, Direct simulation of phonon-mediated heat transfer in a Debye crystal, J. Heat Transfer **116**, 815 (1994).
[43] S. Bosi and C. Jacoboni, Monte Carlo high-field transport in degenerate GaAs, J. Phys. C **9**, 315 (1976).
[44] P. Lugli and D. Ferry, Degeneracy in the ensemble Monte Carlo method for high-field transport in semiconductors, IEEE Trans. Electr. Devices **32**, 2431 (1985).
[45] J.-P. M. Péraud, Low Variance Methods for Monte Carlo Simulation of Phonon Transport, M.Sc. thesis, Massachusetts Institute of Technology, 2011.
[46] Q. Hao, G. Chen, and M.-S. Jeng, Frequency-dependent Monte Carlo simulations of phonon transport in two-dimensional porous silicon with aligned pores, J. Appl. Phys. **106**, 114321 (2009).
[47] A. Jansen, F. Mueller, and P. Wyder, Direct measurement of electron-phonon coupling $\alpha 2F(\omega)$ using point contacts: Noble metals, Phys. Rev. B **16**, 1325 (1977).
[48] S. D. Brorson, A. Kazeroonian, J. S. Moodera, D. W. Face, T. K. Cheng, E. P. Ippen, M. S. Dresselhaus, and G. Dresselhaus, Femtosecond Room-Temperature Measurement of the Electron-Phonon Coupling Constant Gamma in Metallic Superconductors, Phys. Rev. Lett. **64**, 2172 (1990).
[49] D. Gall, Electron mean free path in elemental metals, J. Appl. Phys. **119**, 085101 (2016).
[50] T. Rangel, D. Kecik, P. E. Trevisanutto, G. M. Rignanese, H. Van Swygenhoven, and V. Olevano, Band structure of gold from many-body perturbation theory, Phys. Rev. B **86**, 125125 (2012).
[51] J. E. Turney, A. J. H. McGaughey, and C. H. Amon, In-plane phonon transport in thin films, J. Appl. Phys. **107**, 024317 (2010).
[52] X. Ran, Y. Guo, and M. Wang, Interfacial phonon transport with frequency-dependent transmissivity by Monte Carlo simulation, Int. J. Heat Mass Transfer **123**, 616 (2018).